Journal of Applied Mechanics and Technical Physics, Vol. 45, No. 6, pp. 794–798, 2004

EFFECT OF A SHOCK PULSE ON A FLOATING ICE SHEET

V. M. Kozin and A. V. Pogorelova

UDC 624.124:532.595

The vibrations of a viscoelastic plate lying on an elastic liquid base subjected to pulse loading have been studied theoretically and experimentally. The effect of the variable depth of the reservoir, plate thickness, and strain relaxation time on the value of the plate vibration amplitude and the length and curvature of the flexural gravity wave profile are analyzed. Good agreement of theoretical and experimental results is obtained.

Key words: *pulsed load, flexural gravity wave, disintegration of an ice sheet.*

1. The theoretical part of the present study is devoted to extending the results obtained in [1]. We consider an initially unstrained, homogeneous, isotropic, viscoelastic ice plate lying on an elastic liquid base. The plate is in the state of rest and is loaded by a shock pulse Y at the time $t = 0$. The coordinate system is arranged as follows: the origin is at the point of application of the pulse, the plane xOy coincides with the unperturbed plate–liquid interface, and the z axis points upward. The flow of the fluid of density ρ_2 is assumed to be potential.

According to [2, 3], ice is described by the law of deformation of an elastically delayed, linear Kelvin–Voigt medium [4]. In this case, the differential equation of small vibrations of the floating plate is written as follows (see [1]):

$$\frac{Gh^3}{3}\Big(1+\tau_\phi\frac{\partial}{\partial t}\Big)\nabla^4 w+\rho_1 h\frac{\partial^2 w}{\partial t^2}+\rho_2 g w+\rho_2\frac{\partial\Phi}{\partial t}\Big|_{z=0}=Y\delta(\boldsymbol{r})\delta(t). \tag{1.1}$$

Here $G = 0.5E/(1+\nu)$ is the shear elastic modulus of ice, E is the elastic modulus of ice in tension and compression, ν is Poisson's constant, $h(x, y)$ is the ice thickness, $\rho_1(x, y)$ is the ice density, τ_ϕ is the strain relaxation time for the ice plate or the "delay time" [2–4], $w(x, y, t)$ is the liquid surface strain or the vertical displacement of ice, $\Phi(x, y, z, t)$ is the liquid velocity potential function, which satisfies the Laplace equation ($\Delta\Phi = 0$), $\delta(\boldsymbol{r})$ is the Dirac delta function, $\boldsymbol{r} = (x, y)$ is the radius vector of the current point of the ice surface, and $\delta(t)$ is the Dirac delta function. It is subsequently assumed that ρ_1 and h are constants. As calculated values of the shear modulus G and the density of the plate ρ_1, one should take their reduced values determined as integral values over the plate thickness [2].

The initial conditions for w are homogeneous [1, 2]:

$$w = 0, \qquad \dot{w} = 0 \qquad \text{at} \quad t = 0.$$

The linearized kinematic condition on the ice–water interface has the form [2]

$$\frac{\partial\Phi}{\partial z}\Big|_{z=0}=\frac{\partial w}{\partial t}. \tag{1.2}$$

For the liquid velocity potential function $\Phi(x, y, z, t)$, the boundary condition at the bottom of the reservoir is written as

$$\frac{\partial\Phi}{\partial\boldsymbol{n}}=0 \qquad \text{at} \quad z=-H, \tag{1.3}$$

Institute of Machine Science and Metallurgy, Far East Division, Russian Academy of Sciences, Komsomol'sk-on-Amur 681005; sasha@imim.ru. Translated from Prikladnaya Mekhanika i Tekhnicheskaya Fizika, Vol. 45, No. 6, pp. 26–30, November–December, 2004. Original article submitted November 19, 2003; revision submitted March 22, 2004.

where $\boldsymbol{n}$ is the normal vector to the bottom surface, $H = H_1 + \alpha r - b$, H_1 is the reservoir depth, r is the modulus of the radius-vector $\boldsymbol{r}$, $b = \rho_1 h/\rho_2$ is the ice immersion in static equilibrium, and α is the slope of the bottom surface along the direction of the radius-vector $\boldsymbol{r}$. If $\alpha = 0$, the distance from the ice–water interface to the bottom of the reservoir is constant and equal to $H_1 - b$. If $\alpha > 0$, the depth increases in the direction of the radius-vector $\boldsymbol{r}$, and if $\alpha < 0$, it decreases.

By analogy with [1], to solve the problem, we use Fourier transformation over the coordinates x and y for the functions $w(x, y, t)$ and $\Phi(x, y, z, t)$ and pass to their transforms $w_F(\boldsymbol{\gamma}, t)$ and $\Phi_F(\boldsymbol{\gamma}, z, t)$ in vector form:

$$w(\boldsymbol{r}, t) = \frac{1}{2\pi} \int\limits_{\boldsymbol{\gamma}} \exp\left(i(\boldsymbol{\gamma}\boldsymbol{r})\right) w_F(\boldsymbol{\gamma}, t)\, d\boldsymbol{\gamma}, \qquad \Phi(\boldsymbol{r}, z, t) = \frac{1}{2\pi} \int\limits_{\boldsymbol{\gamma}} \exp\left(i(\boldsymbol{\gamma}\boldsymbol{r})\right) \Phi_F(\boldsymbol{\gamma}, z, t)\, d\boldsymbol{\gamma}$$

$$(\Phi_F(\boldsymbol{\gamma}, z, t) = A_1 \exp(-\gamma z) + B_1 \exp(\gamma z)).$$

Here A_1 and B_1 are unknown functions of the variables $\boldsymbol{\gamma}$ and t and γ is the modulus of the vector $\boldsymbol{\gamma}$.

After applying Fourier transformation to Eq. (1.1) and using the kinematic (1.2) and boundary (1.3) conditions, we obtain the following second-order linear differential equation for w_F with constant coefficients:

$$\ddot{w}_F m(\gamma) + \dot{w}_F k(\gamma) + w_F c(\gamma) = Y\delta(t), \tag{1.4}$$

where

$$k(\gamma) = \tau_\phi \frac{Gh^3\gamma^4}{3}; \qquad m(\gamma) = \rho_1 h + \frac{\rho_2(1+\alpha^2)}{\gamma(\tanh(\gamma H) + \alpha^2 \coth(\gamma H))}; \qquad c(\gamma) = \rho_2 g + \frac{Gh^3\gamma^4}{3}.$$

Applying the Laplace transformation to the solution of Eq. (1.4) under homogeneous initial conditions, we obtain

$$w_F = \begin{cases} \dfrac{Y}{\sqrt{cm - k^2/4}} \exp\Big(-\dfrac{kt}{2m}\Big) \sin\Big(\dfrac{t}{m}\sqrt{cm - \dfrac{k^2}{4}}\Big), & cm - \dfrac{k^2}{4} > 0, \\ \dfrac{Y}{\sqrt{k^2/4 - cm}} \exp\Big(-\dfrac{kt}{2m}\Big) \sinh\Big(\dfrac{t}{m}\sqrt{\dfrac{k^2}{4} - cm}\Big), & \dfrac{k^2}{4} - cm > 0, \\ \dfrac{Y}{m}\, t \exp\Big(-\dfrac{kt}{2m}\Big), & cm - \dfrac{k^2}{4} = 0. \end{cases} \tag{1.5}$$

By analogy with [2], the sought function w is found using the inverse Fourier transformation:

$$w(r, t) = \frac{1}{2\pi} \int\limits_0^\infty w_F \gamma J_0(\gamma r)\, d\gamma. \tag{1.6}$$

The value of w_F is calculated by formulas (1.5), $J_0(\gamma r)$ is the first-order Bessel function, r is the distance from a point to the place of application of the shock pulse, t is time, the values of c, m, and k are calculated by formulas (1.4).

2. The experiments were performed in a reservoir with dimensions $L \times B \times H = 2.0 \times 1.5 \times 1.2$ m. A polymer plate 1 mm thick was used as the model plate. An upward shock pulse was applied by means of a mechanical loading device. The parameters of the modeled waves were measured using a displacement pickup and a two-coordinate plotter. The pulse intensity was chosen depending on the sensitivity of the pickup to ensure stable and reliable recording of plate strain curves. A 20–30% increase in the pulse intensity led to a linear increase in the wave amplitude with an unchanged period.

The measured strains of the plate at distances of 0.26 and 0.52 m are shown by solid curves in Fig. 1a and b, respectively. This location of the pickup relative to the point of pulse application ensured high-quality recording of the wave profile within approximately two wave periods without distortion, i.e., without superposition of the waves reflected from the reservoir walls.

3. The results of calculations by formula (1.6) were compared with the experimental data obtained for the following parameters of the plate and water: $\rho_1 = 2200$ kg/m^3, $\rho_2 = 1000$ kg/m^3, $E = 4.1 \cdot 10^6$ N/m^2, $\nu = 0.45$, $h = 0.001$ m, $\alpha = 0$, $H = 1.2$ m, $\tau_\phi = 5$ sec, and $Y = 4$ kg/sec. The relaxation time of the polymer plate τ_ϕ was chosen so that the periods of the flexural gravity wave in the experiment and calculations were approximately identical. We note that the best agreement of theoretical and experimental data was observed for $\tau_\phi = 5$ sec. Since

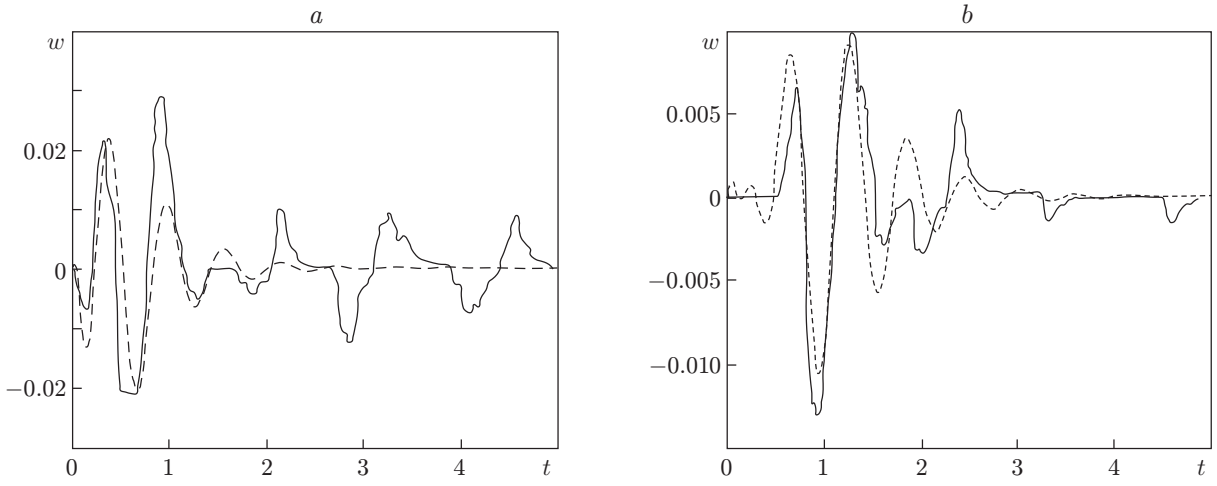

Fig. 1

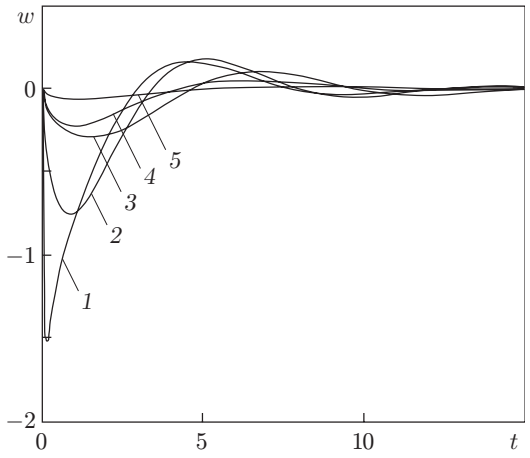

Fig. 2

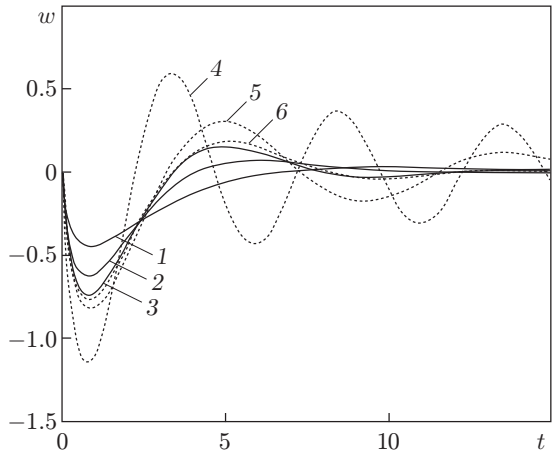

Fig. 3

under the conditions of the experiment, it was not possible to measure the value of the pulse applied to the plate, in calculations by formula (1.6), we used the value of the pulse for which the theoretical and experimental vibration frequencies of the plate are approximately equal. Figure 1 shows the results of calculations by formula (1.6) (dashed curves) and experimental data (solid curves) for distances of 0.26 and 0.52 m from the pulse source. It obvious that solution (1.6) for the viscoelastic model of the plate is correct and agree well with the experimental data for $t \leqslant 1.5$ sec, i.e., for the time interval in which the effect of reflected waves is ignored in measurement results.

4. In the calculations using formula (1.6), the distances to the point of pulse application, the time elapsed from the moment of pulse application, the reservoir depth, the ice plate thickness, and the relaxation time were varied and the ice and water parameters were as follows: $\rho_1 = 900$ kg/m^3, $\rho_2 = 1000$ kg/m^3, $E = 5 \cdot 10^9$ N/m^2, $\nu = 1/3$, and $Y = -10^7$ kg/sec. The ice thickness h was varied from 0.1 to 2.0 m, the relaxation time τ_ϕ from 0.001 to 10 sec, the distance from the ice–water interface to the bottom H from 1 m to infinity, and the slope of the bottom surface α from -1 to 1.

Figure 2 shows curves of $w(t)$ at the point of pulse application $r = 0$ for $H = 100$ m, $\alpha = 0$, and various values of the relaxation time τ_ϕ and ice thickness h. Curves 1–3 correspond to $\tau_\phi = 0.05$, 0.69, and 5 sec for $h = 0.5$ m. It is evident that an increase in the relaxation time leads to a decrease in the amplitude and an increase in the plate

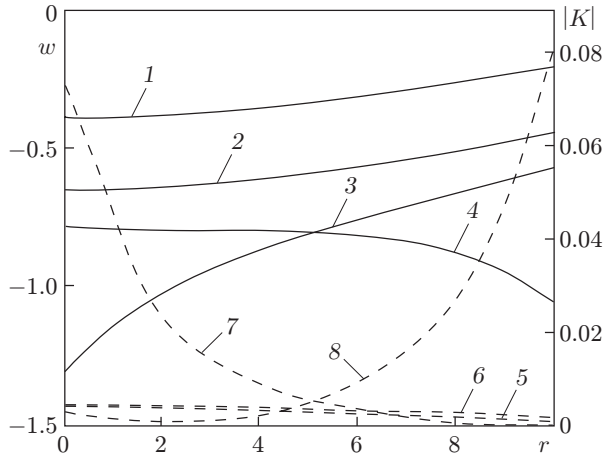

Fig. 4

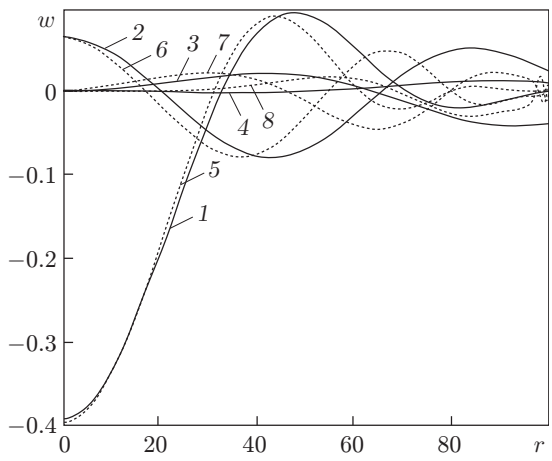

Fig. 5

vibration period. In [5, 6], it is shown that the viscoelastic model of ice gives the best fit to the experimental data for a relaxation time $\tau_\phi = (0.690 \pm 0.067)$ sec. Curves 2, 4, and 5 correspond to plate thicknesses $h = 0.5$, 1, and 2 m at $\tau_\phi = 0.69$ sec. As one might expect, an increase in the plate thickness results in a decrease in the plate deflection amplitude and an increase in the wavelength and period.

Figure 3 shows the effect of the slope of the bottom surface α on the vertical displacement of the plate w for various H versus time t at the point of pulse application $r = 0$ for $\tau_\phi = 0.69$ sec and $h = 0.5$ m. Curves 1–3 refer to $H_1 - b = 30$, 10, and 3 m for $\alpha = 0$ and curves 4–6 refer to the same values of $H_1 - b$ for $\alpha = \pm 1$. From Fig. 3 it is evident that the slope of the bottom surface leads in an increase in the plate deflection amplitude. The smaller the reservoir depth, the stronger the effect of α on the deflection of the ice plate.

Figure 4 shows the effect of the reservoir depth and the slope of the bottom surface on the value of w and the modulus of the bending curvature of the ice surface $|K|$ versus the distance r from the point of pulse application at the time $t = 0.7$ sec for $\tau_\phi = 0.69$ sec and $h = 0.5$ m. Curves 1 and 2 are plots of the dependence $w(r)$ for $H = 2$ and 12 m, respectively ($\alpha = 0$). Curves 5 and 6 show the dependences of the curvature modulus on radius for curves 1 and 2, respectively. It is evident that an increase in the reservoir depth results in an increase in the deflection of the ice plate in the neighborhood of the loading point and to an insignificant increase in the bending curvature of the plate. Curves 3 and 4 are plots of the dependence $w(r)$ for $H_1 - b = 2$ m and $\alpha = 1$ and $H_1 - b = 12$ m and $\alpha = -1$, respectively, curves 7 and 8 are plots of the curvature modulus versus radius for curves 3 and 4. From the results presented in Fig. 4 (curves 3, 4, 7, and 8), it follows that an inclined bottom and a shallow depth can result in a factor of 5–10 increase in the bending curvature of the ice surface. We note that curves 3 and 4 in Fig. 4 refer to large values of the slope angle ($\alpha \approx 1$) in the case where the distance from deep to shallow water is much smaller than the length of the flexural gravity wave.

Figure 5 shows the effect of a small slope angle of the bottom surface ($\alpha \ll 1$) and time t on the vertical displacement of the ice plate w for $h = 0.5$ m, $\tau_\phi = 0.69$ sec, and $H_1 - b = 11$ m. Curves 1–4 refer to $t = 2$, 5, 10, and 15 sec for a constant depth ($\alpha = 0$). An analysis of these curves shows that the largest deflection of the ice plate is attained at initial times in the neighborhood of the point of pulse application. Curves 5–8 show development of a flexural gravity wave under conditions of a small elevation of the bottom surface ($\alpha = -0.109$) at the times $t = 2$, 5, 10, and 15 sec, respectively. It can be seen that as the wave reaches a shallow depth of 0.1 m, which corresponds to $r = 100$ m for $\alpha = -0.109$, the flexural gravity wave is "compressed," i.e., its length decreases. From the calculations, it follows that in the neighborhood of $r = 100$ m, the curvature increases by a factor of several hundred with time.

The results of this study can be used to estimate the ice-breaking capacity of flexural-gravity waves produced by shock pulses.

REFERENCES

1. V. M. Kozin and A. V. Pogorelova, "Deformation of an infinite ice plate caused by a shock pulse," in: *Proc. Int. Symp. on Problem of Sciences, Engineering, and Education*, Vol. 3, Academy of Earth Sciences, Moscow (2002), pp. 48–50.
2. D. E. Kheisin, *Dynamics of an Ice Sheet* [in Russian], Gidrometeoizdat, Leningrad (1967).
3. V. M. Kozin and A. V. Pogorelova, "Wave resistance of amphibian aircushion vehicles moving on ice fields," *J. Appl. Mech. Tech. Fiz.*, **44**, No. 2, 193–199 (2003).
4. A. Freudental and H. Geiringer, *The Mathematical Theories of the Inelastic Continuum*, Springer Verlag, Berlin–Göttingen–Heidelberg (1958).
5. V. A. Squire, R. J. Hosking, A. D. Kerr, and P. J. Langhorne, *Moving loads on ice plates*, Kluwer Acad. Publ., Dordrecht (1996).
6. T. Takizava, "Deflection of a floating sea ice sheet induced by a moving load," *Cold Regions Sci. Technol.*, **11**, 171–180 (1985).